Theor Chem Account (2008) 119:69–79
DOI 10.1007/s00214-007-0284-8

REGULAR ARTICLE

Reduction of linear birefringence in vibrational circular dichroism measurement: use of a rotating half-wave plate

Xiaolin Cao · Rina K. Dukor · Laurence A. Nafie

Received: 20 May 2006 / Accepted: 20 March 2007 / Published online: 21 April 2007

Abstract A new method has been developed to suppress the effects of linear birefringence (LB) associated with sample cells in the measurement of vibrational circular dichroism (VCD) spectra by adding a rotating half-wave plate (RHWP) to the optical train. The method functions in combination with the previously developed dual polarization modulation (DPM) technique and involves placing the RHWP after the second photo-elastic modulator (PEM) of the DPM setup. In the DPM setup without the RHWP, all sources of LB terms are first reduced and then further cancelled by real time electronic subtraction, except for one remaining LB term associated with sample cell. Not infrequently, however, this remaining source of LB between the two PEMs with axes at 45° relative to the stress axes of the PEMs leads to noticeable deviations of the VCD baseline that cannot be eliminated. The new method described here depends on the use of an achromatic half-wave plate which is currently available in the near-infrared region with a low-frequency cut off near 2, 000 cm^{-1}. It is demonstrated theoretically, and experimentally in the CH stretching region, that the addition of a RHWP eliminates this last remaining source of LB from the VCD measurement.

Electronic supplementary material The online version of this article (doi:10.1007/s00214-007-0284-8) contains supplementary material, which is available to authorized users.

X. Cao · L. A. Nafie
Department of Chemistry, Syracuse University,
Syracuse, NY 13244, USA

R. K. Dukor · L. A. Nafie (✉)
BioTools Inc., 17546 Beeline Hwy,
Jupiter, FL 33548, USA
e-mail: Lanafie@aol.com

X. Cao
Department of Global Cellular and Analytical Resources,
Amgen Inc. Thousand Oaks, CA 91320, USA

Keywords Vibrational circular dichroism (VCD) · Linear birefringence (LB) · Rotating half-wave plate (RHWP) · Dual polarization modulation (DPM)

1 Introduction

Vibrational circular dichroism (VCD) is an extension of electronic CD to vibrational transitions. It is defined as the differential absorbance (ΔA) of left and right circularly polarized (LCP and RCP) infrared radiation by a molecule with chirality during vibrational excitation [1–4]. The VCD intensity is low and is usually in the range of 10^{-4}–10^{-5} absorbance units [3,4]. As such, one of the primary concerns in the measurement of VCD spectra is the reduction of optical artifacts that interfere with typically small VCD intensities. One major form of artifacts is called baseline artifacts [5], which usually originate from strain and polarization sensitivity and other imperfections of optical components throughout the optical train. The strain existing in optics manifests itself as linear birefringence (LB) which alters the beam polarization state and results in baseline artifacts. Over the years, many attempts have been undertaken to reduce artifacts associated with LB [5–11]. These artifacts can be reduced or eliminated by acquiring VCD baselines for no sample cell in the beam, an empty sample cell in the beam, a sample cell with an achiral sample, such as the solvent or a solution of the racemic mixture, or a solution of the opposite enantiomer of the chiral sample molecule. Of these, the best way to determine the baseline offset spectrum is to measure a VCD spectrum of the racemic mixture or the opposite enantiomer of a chiral sample under identical conditions. Frequently, if neither the opposite enantiomer nor the racemic mixture is available, the baseline may be corrected by subtracting the solvent VCD spectrum measured under the same experimental conditions.

However, the solvent baseline correction does not ensure that an artifact-free VCD spectrum will be obtained since the sample and solvent have different optical properties, which may result in different VCD baselines.

In addition to these sampling methods for artifact reduction, a number of methods have been investigated over the years to reduce artifacts by optical–electronic or purely optical methods. The earliest of these is the method of polarization scrambling in which a second photo-elastic modulator (PEM) is used in a dispersive wavelength-scanning spectrometer [6]. This method achieves artifact cancellation at one particular wavelength in the IR spectrum, and this wavelength location is synchronized to the scanning wavelength monochromator as the VCD spectrum is recorded. This method falls short of complete cancellation for Fourier transform (FT) VCD measurements since all wavelengths are recorded simultaneously for a single PEM setting. Other methods of artifact reduction reported have included polarization demodulation [7], the use of lenses instead of mirrors for the focusing the IR beam to the detector [8,9], the use of a rotating quarter-wave plate [10], and theoretical simulations using a rotating polarizer [11].

A few years ago, a real time spectral-multiplex method called dual polarization modulation (DPM) was proposed by Nafie [5] to reduce and eliminate LB artifacts in the optical train of an FT-VCD spectrometer. The DPM method involves adding a second PEM to the optical train between the sample and the detector. In this setup, two VCD spectra are measured simultaneously using the two PEMs, one placed before and one after the sample. These two VCD spectra are then subtracted electronically in real time to cancel LB terms when the second PEM is properly adjusted [5]. For the DPM setup, several different optical arrangements were discussed. These include dual polarization modulation with or without a second polarizer and multiple polarization modulation where a third or a fourth PEM is added in the optical train. The aim of adding a second polarizer in the DPM setup is to control the polarization state of the light reaching the detector and thereby provide a way for total and complete cancellation of all LB artifacts. However, this strategy works at the cost of magnifying the LB terms by two orders of magnitude compared to the DPM setup without a second polarizer. In practice, it is found that the exact cancellation of magnified LB terms is difficult to realize and cancellation inaccuracies lead to significant LB artifacts in the VCD spectra. Adding a third or even a fourth PEM in the optical train is complicated and expensive relative to their effectiveness in suppressing LB artifacts. As such, the DPM setup without a second polarizer has been found to be the most practical way to reduce and cancel the major LB terms. However, this method does not reduce or cancel any source of LB located between the two PEMs for which birefringence axes are at 45° from the PEM axes. This location is typically where a sample cell is placed for VCD measurement. This LB source is negligible only if the sample cell is optically uniform and has little strain, or it can be ignored if the polarization sensitivity of the detector is low or its polarization bias is very close to vertical or horizontal. Unfortunately, in most cases the polarization sensitivity of the detector is difficult to control and the sample cells are not free of strain, and thus unwanted LB from sample cells is often observed in VCD spectra.

More recently, Hug [12] proposed a procedure to eliminate optical offsets by subtracting an optical activity spectrum of one chiral molecule from that of its "virtual enantiomer", and the method is demonstrated for the measurement of scattered circular polarization (SCP) Raman optical activity (ROA). The virtual enantiomer method involves introduction of two half-wave plates (HWPs), one placed before and another after a chiral sample to create its "virtual enantiomer". The ROA spectra of both the molecule and its "enantiomer" can be collected and subsequently subtracted to obtain an offset-free spectrum. This technique resembles the enantiomeric correction methods mentioned above and works very well in ROA spectroscopy and has a significant advantage: no real enantiomer is needed for baseline correction. The practical implementation of the method utilized rotating half-wave plates, referred to as linear rotators. The linear rotators time-average to zero any linear polarization components of the light that may be present in the optical train. In particular, the effects of any LB associated with the sample cell that produces linearly polarized light from circularly polarized light is time-averaged to zero. The SCP-ROA experiments of Hug [12] clearly demonstrate that it is possible to carry out measurements in a way that eliminates offsets that might occur through the influence of the differing chiroptical properties of the two chiral antipodes.

However, the "virtual enantiomer" technique demonstrated in ROA measurements is more difficult to realize in VCD measurements due to the wide range of spectral frequencies spanned by IR spectra. Moreover, if the sample possesses LB, such as a strained optical cell, the two stationary HWPs may not be able to create an identical virtual enantiomer for baseline correction. The initial experimental tests show that the identical "virtual enantiomer" is indeed difficult to create in VCD measurements. Nevertheless, we have found that the augmentation of using a linear rotator, or rotating half-wave plate (RHWP), similar to that used by Hug [12] has a very satisfactory outcome.

In this study, we consider the effect of a RHWP placed between the sample cell and the detector for VCD measurements. As in the case of ROA measurements discussed above, the fundamental effect of the RHWP, aside from reversing the circularity of the polarization state, is to average to zero any linear polarization components present in the beam due to LB prior to the RHWP. As shown in the following discussions, placement of a RHWP after the second PEM in a

DPM setup can eliminate LB originating in the sample cell between the two PEMs, which includes the only source of LB that is immune to the action of the DPM setup. As a consequence, we are able to show that the RHWP and DPM methods are complementary approaches and their combined use is an effective approach to reduce close to zero all LB effects throughout the optical train.

VCD measurements have been performed using camphor in CCl_4 solution with two different sample cells and at various optical settings of the DPM and the RHWP. Theoretical analyses of the mechanisms of LB reduction and cancellation are carried out via Stokes–Muller matrix formalism and confirmed by experimental results in the hydrogen-stretching region.

We note here that a RHWP has been used previously for the elimination of linear components in light beams when the measurement of pure circular polarization has been carried out. In addition to the use of RHWPs in ROA measurements by Hug [12], a RHWP has been used previously in astronomical applications for the measurement of circular polarization content of starlight [13]. Although not formally published to our knowledge, the use of a RHWP has been included in the design of ROA spectrometers constructed at the Glasgow University by Barron and Hecht [14].

2 Experimental

All VCD and IR spectra were measured at a resolution of $16\,cm^{-1}$ in the CH-stretching region from about 4,000 to $2,000\,cm^{-1}$. The measurements were carried out on Chiral *IR* FT-VCD spectrometer from BioTools Inc. (www.btools.com), Jupiter, FL. The spectrometer was modified to have an external bench to facilitate the setup of DPM [5] and a RHWP. Two CaF_2 photo-elastic modulators (PEM) from Hinds Instrument, Inc. (www.hindspem.com), Hillsboro, OR, operating at different frequencies in the range of 57 kHz were set for maximum quarter-wave retardation efficiency at $3,000\,cm^{-1}$. The FT-VCD spectrometer uses two tungsten/halogen lamps as the sources [15] and is equipped with a thermoelectric (TE) cooled MCT detector [3]. A band-pass optical filter from 4,000 to $2,000\,cm^{-1}$ was used in front of the first PEM to avoid detector saturation and permit maximum electronic throughput and thus signal-to-noise ratio in the measured spectral range. The optical filter was obtained from Spectrogon US, Inc. (www.spectrogon.com), Parsippany, NJ.

The DPM electronic units used for the FT-VCD spectrometer system include a dual-channel digital electronic filter, Model SR-650, and two DSP Model SR-830 lock-in amplifiers (LIAs) that were tuned to the two PEM frequencies, respectively. Both the electronic filter and LIAs are from Stanford Research Systems (www.thinksrs.com) Sunnyvale, CA. All the measurements were performed by use of a software routine, Chiral*IR*®, which is part of the BGrams 32® program package. A super achromatic zeroth-order half-wave ($\lambda/2$) plate was obtained from B. Halle Nachfolger (www.b-halle.de), Berlin, Germany. This achromatic $\lambda/2$ plate consists of three pieces of double layer, uncoated MgF_2 plates with a thickness of about 0.8 mm. All the plates are optically contacted and have dimensions of about 20 × 20 mm. The HWP works in a range from 2.5 to ca 4.5 μm (4,000 to 2, $200\,cm^{-1}$) with an estimated less than 1% deviation from $\lambda/2$ in the spectral range of the interest. The HWP was confined in a circular metal holder to form a circular window 20 mm in diameter. It is driven by a mini motor-assembly obtained from MicroMo Electronics, Inc. (www.micromo.com), Clearwater, FL. The mini motor-assembly has a voltage controller to adjust the rotation speed of the RHWP, which was set to near 60 cycles per minute for the RHWP experiments reported here.

Samples of *R*-(+)-camphor and *S*-(−)-camphor were obtained from Aldrich Chemical Co. and used without further purification. At room temperature camphor is a white solid and is highly soluble in CCl_4. Camphor has been used widely to evaluate instrument performance in the mid-IR due to its VCD spectrum near $3,000\,cm^{-1}$ where it has a prominent and distinct VCD couplet. Moreover, the anisotropy ratio of this couplet is on the order of magnitude of 10^{-5}, which is typical for molecules in this region. In this study, camphor was dissolved in CCl_4 at two different concentrations, 0.3 and 0.6 M, used in two IR liquid cells with pathlengths of 0.10 and 0.05 mm, respectively. The two liquid BaF_2 cells have a circular window of 20 mm in diameter and were obtained from ICL (International Crystal Laboratory), Garfield, NJ. These two combinations of solution concentrations and cell pathlengths were used to obtain a desired absorbance range in the sample from 0.3 to 0.8 for optimal VCD signal-to-noise (SNR) ratios. All the VCD spectra reported were measured with a collection time of 1 h.

3 Theoretical analysis

As mentioned above, the methodology used for the reduction of LB is to introduce a RHWP into the optical beam, separately or in combination with the DPM setup. The basic DPM setup has a second PEM in the optical train, located behind sample, and it can be represented as the following configuration:

$$S_p \rightarrow \text{PEM1} \rightarrow \text{X} \rightarrow \text{PEM2} \rightarrow \text{DTC} \rightarrow S_D \qquad \text{(I)}$$

where S_p symbolizes the incident infrared beam, PEM1 and PEM2 represent the two photo-elastic modulators, X stands for the chiral sample and DTC for the detector. Finally, S_D

represents the intensity of the radiation at the detector. Infrared radiation is emitted from a tungsten/halogen lamp inside the FT-VCD spectrometer and is linearly polarized before it reaches the first PEM, which is used to modulate linearly polarized light between left- and right-circularly polarized light at the frequency, ω_{M}. The differential absorbance for LCP and RCP for a chiral sample is defined as $\Delta A(\tilde{\nu}) = A_{\mathrm{L}}(\tilde{\nu}) - A_{\mathrm{R}}(\tilde{\nu})$, where $\tilde{\nu}$ is the radiation frequency in wavenumbers. To calculate the total beam intensity received by the detector, we apply Stokes–Muller matrix formalism [5] to describe the beam transformations by the various components on the optical train. The Stokes vector of the infrared beam for vertically polarized radiation is given by

$$S_{\mathrm{P}} = I_0(\tilde{\nu}) \times \begin{bmatrix} 1 \\ 1 \\ 0 \\ 0 \end{bmatrix} \tag{1}$$

where $I_0(\tilde{\nu})$ is the light intensity, a function of frequency $\tilde{\nu}$, and the four entries from top to bottom represent the total intensity, the differential intensity of vertical minus horizontal linearly polarized light, the differential intensity of $+45°$ minus $-45°$ linearly polarized light, and finally the differential intensity between RCP minus LCP light. The sense of all positive angles is taken to be positive in the clockwise direction when looking from the detector back to the source. The Mueller matrices for the two PEMs are represented as M_{PEM1} and M_{PEM2}, respectively [5]

$$M_{\mathrm{PEM}i}(\tilde{\nu}) = \begin{bmatrix} 1 & 0 & 0 & 0 \\ 0 & \cos\delta_{Mi}(\tilde{\nu}) & 0 & -\sin\delta_{Mi}(\tilde{\nu}) \\ 0 & 0 & 1 & 0 \\ 0 & \sin\delta_{Mi}(\tilde{\nu}) & 0 & \cos\delta_{Mi}(\tilde{\nu}) \end{bmatrix}, \quad i = 1, 2 \tag{2}$$

where δ_{M_i} is the phase angle function of the PEM that itself oscillates sinusoidally in time at the PEM frequency ω_{M}:

$$\delta_{Mi}(\tilde{\nu}) = [\delta^0_{Mi}(\tilde{\nu})] \sin\omega_{Mi} t \tag{3}$$

where $\delta^0_{\mathrm{M}_i}(\tilde{\nu})$ is the maximum retardation angle of the polarization modulation cycle at each frequency $\tilde{\nu}$. The Mueller matrix, M_X, of a chiral sample X with absorbance $A(\tilde{\nu}) = \frac{1}{2}\left[A_{\mathrm{L}}(\tilde{\nu}) + A_{\mathrm{R}}(\tilde{\nu})\right]$, is represented as [5]

$$M_X = 10^{-A(\tilde{\nu})} \begin{bmatrix} 1 & 0 & 0 & 1.1513\Delta A(\tilde{\nu}) \\ 0 & 1 & 0 & 0 \\ 0 & 0 & 1 & 0 \\ 1.1513\Delta A(\tilde{\nu}) & 0 & 0 & 1 \end{bmatrix} \tag{4}$$

where $\Delta A(\tilde{\nu})$ is the differential absorbance defined above. The coefficient 1.1513 is equal to (ln 10)/2 as a result of the change of exponential base.

The semi-conductor detectors used in VCD measurements have been shown to possess mild sensitivity to the linear polarization state of light [6]. As a result, we treat the detector as a polarizer (P) with efficiency ε, where ε is a small coefficient, of the order of 10^{-2} in magnitude. This is equivalent to writing the Muller matrix of a detector as $M_{\mathrm{DTC}} = M_{\mathrm{I}} + 2\varepsilon M_{\mathrm{P}}$, where M_{I} is a unit matrix and M_{P} is the Muller matrix of an ideal polarizer and the factor of 2 is introduced for simplicity of representation. Therefore the Muller matrix of the polarization sensitivity of the detector can be represented as

$$M_{\mathrm{DTC}} = \begin{bmatrix} 1 & \varepsilon\cos\theta & \varepsilon\sin\theta & 0 \\ \varepsilon\cos\theta & 1+\varepsilon\cos^2\theta & \varepsilon\sin\theta\,\cos\theta & 0 \\ \varepsilon\sin\theta & \varepsilon\sin\theta\,\cos\theta & 1+\varepsilon\sin^2\theta & 0 \\ 0 & 0 & 0 & 1 \end{bmatrix} \tag{5}$$

where $\theta = 2\phi$, and ϕ is the angle of polarization axis relative to the vertical, where again positive values correspond to the clockwise direction when viewing radiation coming toward the observer from the source.

The matrix representation of linear birefringence plate (BP) is determined by two parameters, the retardation angle $\delta_{\mathrm{B}}(\tilde{\nu})$ and the angle α of its fast axis [5] of birefringence with respect to the laboratory vertical direction. The Muller matrix representation M_{B} of a general BP is written as

$$M_{\mathrm{B}}(\tilde{\nu}) = \begin{bmatrix} 1 & 0 & 0 & 0 \\ 0 & \cos^2 2\alpha + \sin^2 2\alpha\cos\delta_{\mathrm{B}}(\tilde{\nu}) & \cos 2\alpha\,\sin 2\alpha(1-\cos\delta_{\mathrm{B}}(\tilde{\nu})) & -\sin 2\alpha\,\sin\delta_{\mathrm{B}}(\tilde{\nu}) \\ 0 & \cos 2\alpha\,\sin 2\alpha(1-\cos\delta_{\mathrm{B}}(\tilde{\nu})) & \sin^2 2\alpha + \cos^2 2\alpha\,\cos\delta_{\mathrm{B}}(\tilde{\nu}) & \cos 2\alpha\,\sin\delta_{\mathrm{B}}(\tilde{\nu}) \\ 0 & \sin 2\alpha\,\sin\delta_{\mathrm{B}}(\tilde{\nu}) & -\cos 2\alpha\,\sin\delta_{\mathrm{B}}(\tilde{\nu}) & \cos\delta_{\mathrm{B}}(\tilde{\nu}) \end{bmatrix} \tag{6}$$

Linear birefringence of the optical train has a number of origins, such as lenses and windows of the sample cell and detector. For example, measurable LB is typically associated with the sample cell between the two PEMs. LB may also be present between the second PEM and the detector, originating in the window of the detector or the detector focusing lens (both are not shown in (I)). The LB in the VCD optical train is usually small, compared with the LB of a BP plate, such as

a quarter-wave plate ($\delta = \pi/2$, radians) or a half-wave plate ($\delta = \pi$, radians). It is found experimentally that for stray LB in the optical train, δ is of the order of 0.01 rad. Therefore, to a good approximation we can set $\cos[\delta_B(\tilde{\nu})] \simeq 1$ and $\sin[\delta_B(\tilde{\nu})] \approx \delta_B(\tilde{\nu})$ in Mueller matrix for the BP plate in Eq. (6), which becomes simply

$$M_{LB}(\tilde{\nu}) = \begin{bmatrix} 1 & 0 & 0 & 0 \\ 0 & 1 & 0 & -\beta_B(\tilde{\nu}) \\ 0 & 0 & 1 & \beta'_B(\tilde{\nu}) \\ 0 & \beta_B(\tilde{\nu}) & -\beta'_B(\tilde{\nu}) & 1 \end{bmatrix} \tag{7}$$

and where

$$\begin{aligned} \beta_B(\tilde{\nu}) &= \delta_B(\tilde{\nu}) \sin 2\alpha \\ \beta'_B(\tilde{\nu}) &= \delta_B(\tilde{\nu}) \cos 2\alpha \end{aligned} \tag{8}$$

It is seen from Eq. (8) that $\beta_B(\tilde{\nu})$ is sensitive to birefringence with stress axes $\pm 45°$ from the vertical, which are parallel or perpendicular to the PEM stress axes. The term $\beta'_B(\tilde{\nu})$ is sensitive to birefringence with stress axes in the vertical and horizontal directions. Generally, for different optical components, LB may vary both in magnitude and orientation across the optical element. Here we first focus on the LB associated with the sample cell, located between the two PEMs. It has been shown in our previous study [5] that we can express the contribution of a series of consecutive LB sources by a single LB Mueller matrix where only one unprimed and one primed birefringence angle are used.

The Mueller matrix for a RHWP can also be derived using Eq. (6). For a rotating plate the orientation angle α changes continuously and repeatedly from 0 to 2π. Thus its matrix elements are time-averaged over this range of orientation angles. Substituting the matrix elements in Eq. (6) with the integrated values, we can obtain the Mueller matrix, M_{RWP}, for a rotating wave plate (RWP) [5]

$$M_{RWP}(\tilde{\nu}) = \begin{bmatrix} 1 & 0 & 0 & 0 \\ 0 & [1+\cos\delta_{RWP}(\tilde{\nu})]/2 & 0 & 0 \\ 0 & 0 & [1+\cos\delta_{RWP}(\tilde{\nu})]/2 & 0 \\ 0 & 0 & 0 & \cos\delta_{RWP}(\tilde{\nu}) \end{bmatrix} \tag{9}$$

For an RHWP with the retardation angle $\delta = \pi$ and Eq. (9) further reduces to

$$M_{RHWP}(\tilde{\nu}_{\lambda/2}) = \begin{bmatrix} 1 & 0 & 0 & 0 \\ 0 & 0 & 0 & 0 \\ 0 & 0 & 0 & 0 \\ 0 & 0 & 0 & -1 \end{bmatrix} \tag{10}$$

For the achromatic HWP used in this experiment, there are minor deviations from exact half-wave retardation across the spectral region. To a good approximation, these deviations can be ignored.

We have now obtained all the Mueller matrices needed for the VCD optical train. The final intensity at the detector can be calculated by a sequence of Mueller matrix operations representing the optical components of the IR beam, and this is readily accomplished by MathCad© software (2001 Professional), Mathsoft Inc. (www.mathsoft.com), Needham, MA. For simplicity of matrix operations, dimensionless representations of the Stokes vectors and Mueller matrices are used. To do this, first all the coefficients in front of the vectors and matrices are omitted, such as $I_0(\tilde{\nu})$ in Eq. (1) and $10^{-A(\tilde{\nu})}$ in Eq. (4). The constant 1.1513 in the matrix of Eq. (4) may be combined with $\Delta A(\tilde{\nu})$ and recovered in the final expressions if needed. Next the elements of the PEM Mueller matrices in Eq. (2) may be further simplified in the context of the actual electronic setup for VCD measurements. Replacing the retardation angle $\delta_M(\tilde{\nu})$ of the PEM in Eq. (2) with Eq. (3), we have more complex representations of the matrix elements: $\sin[\delta^0_M(\tilde{\nu}) \sin \omega_M t]$ and $\cos[\delta^0_M(\tilde{\nu}) \sin \omega_M t]$. These representations can be expanded to the series of Bessel functions:

$$\begin{aligned} &\sin[\delta^0_M(\tilde{\nu}) \sin \omega_M t] \\ &\quad = 2\sum_n J_n[\delta^0_M(\tilde{\nu})] \sin n\omega_M t, \quad n = 1, 3, 5, \ldots \\ &\cos[\delta^0_M(\tilde{\nu}) \sin \omega_M t] \\ &\quad = J_0[\delta^0_M(\nu)] + 2\sum_n J_n[\delta^0_M(\tilde{\nu})] \sin n\omega_M t, \quad n = 2, 4, 6, \ldots \end{aligned} \tag{11}$$

For the actual VCD setup, the signal from detector is modulated by the PEM and detected by a lock-in amplifier (LIA) that is tuned to the modulation frequency ω_M. Therefore any higher order harmonics ($2\omega_M$, $3\omega_M$, ...) are rejected by the LIAs and only the first harmonic term $\sin\omega_M$ (AC) is detected and amplified. The terms that are constant (DC) with respect to polarization modulation can be directly processed as the transmission spectrum. Thus Eq. (11) simplifies to

$$\begin{aligned} \sin\left[\delta^0_M(\tilde{\nu}) \sin \omega_M t\right] &\to 2J_1\left[\delta^0_M(\tilde{\nu})\right] \\ \cos\left[\delta^0_M(\tilde{\nu}) \sin \omega_M t\right] &\to J_0\left[\delta^0_M(\tilde{\nu})\right] \end{aligned} \tag{12}$$

where J_1 and J_0 represent the first and zeroth-order Bessel functions, respectively. Therefore, the expressions $\sin\delta_M$ and $\cos\delta_M$ in the Mueller matrix of PEM may be replaced with J_1 and J_0 functions, respectively, for matrix operations and in final representations. The J_1 and J_0 Bessel functions of the two PEMs can be distinguished by their variables, $\delta^0_{M1}(\tilde{\nu})$ and $\delta^0_{M2}(\tilde{\nu})$ for PEM1 and PEM2, respectively. For the final representation of intensity we define a dimensionless intensity $i_D(\tilde{\nu})$, such that $I_D(\tilde{\nu}) = i_D(\tilde{\nu}) \times I_0(\tilde{\nu}) 10^{-A(\tilde{\nu})}$, where $I_D(\tilde{\nu})$ is the actual total intensity at the detector.

3.1 DPM setup without RHWP and with one LB source

For this optical train, we show below that one LB source from sample cell remains unaffected by the DPM setup without a RHWP. The optical configuration of this setup is:

$$\mathrm{S_p} \rightarrow \mathrm{PEM1} \rightarrow \mathrm{X} \rightarrow \mathrm{LB} \rightarrow \mathrm{PEM2} \rightarrow \mathrm{DTC} \rightarrow \mathrm{S_D} \quad \text{(II)}$$

where LB is the linear birefringence from sample cell between the two PEMs. This configuration has been investigated in our previous study [5]. It can be shown that the Mueller matrices of M_x and M_{LB} commute with each other due to the fact that the higher order small items, $\Delta A\beta$ and $\Delta A\beta'$ can be ignored, that is

$$M_X M_{\mathrm{LB}} = M_{\mathrm{LB}} M_X = \begin{bmatrix} 1 & 0 & 0 & \Delta A \\ 0 & 1 & 0 & -\beta \\ 0 & 0 & 1 & \beta' \\ \Delta A & \beta & -\beta' & 1 \end{bmatrix} \quad (13)$$

This shows that the location of LB relative to the sample between the two PEMs is not important. Thus the LB in configuration II can be viewed as the total LB between the two PEMs. The final Stokes vector S_{D} is calculated by operating the Muller matrices sequentially on the initial Stokes vector S_{p} according to their location in the optical configuration (II):

$$S_{\mathrm{D}} = M_{\mathrm{DTC}} M_{\mathrm{PEM2}} M_{\mathrm{LB}} M_X M_{\mathrm{PEM1}} S_{\mathrm{P}} \quad (14)$$

The total intensity of the light that reaches the detector is the first entry of the Stokes vector S_{D}, that is

$$\begin{aligned} i_{\mathrm{D}}(\nu) &= i_{\mathrm{DC}}(\tilde{\nu}) + i_{\mathrm{AC1}}(\tilde{\nu}) + i_{\mathrm{AC2}}(\tilde{\nu}) \\ &= 1 + \varepsilon(\theta) J_0\left[\delta^0_{\mathrm{M1}}(\tilde{\nu})\right] J_0\left[\delta^0_{\mathrm{M2}}(\tilde{\nu})\right] \cos\theta \\ &\quad + 2J_1\left[\delta^0_{\mathrm{M1}}(\tilde{\nu})\right]\left\{\Delta A(\tilde{\nu}) + \varepsilon(\theta)\beta'_{\mathrm{M}}(\tilde{\nu}) \sin\theta \right. \\ &\quad \left. - \varepsilon(\theta)\beta_{\mathrm{B}}(\tilde{\nu}) \cos\theta J_0\left[\delta^0_{\mathrm{M2}}(\tilde{\nu})\right]\right\} \\ &\quad - 2J_1\left[\delta^0_{\mathrm{M2}}(\tilde{\nu})\right]\left\{\varepsilon(\theta)\Delta A(\tilde{\nu}) \right. \\ &\quad \left. + \varepsilon(\theta)\beta_{\mathrm{B}}(\tilde{\nu}) J_0\left[\delta^0_{\mathrm{M1}}(\tilde{\nu})\right]\right\} \cos\theta \end{aligned} \quad (15)$$

Here $i_{\mathrm{DC}}(\tilde{\nu})$ represents that part of the detector signal that is not modulated at a PEM frequency. This corresponds to the ordinary FT-IR transmission signal. The detector signals, $i_{\mathrm{AC1}}(\tilde{\nu})$ and $i_{\mathrm{AC2}}(\tilde{\nu})$, represent those parts of the detector signal modulated at the frequencies of the first and second PEMs, respectively, and carry information about the VCD spectrum and the VCD baseline. The detector's polarization sensitivity $\varepsilon(\theta)$ and the LB terms $\beta_{\mathrm{M}}(\tilde{\nu})$ and $\beta'_{\mathrm{M}}(\tilde{\nu})$ are of the order of 10^{-2}, while $\Delta A(\tilde{\nu})$ is of the order of 10^{-4}–10^{-5}. Therefore items such as $\Delta A(\tilde{\nu})\varepsilon(\theta)$, $\Delta A(\tilde{\nu})\beta_{\mathrm{M}}(\tilde{\nu})$, $\Delta A(\tilde{\nu})\beta'_{\mathrm{M}}(\tilde{\nu})$ are higher order small terms and are negligible compared to the magnitude of the terms in $\Delta A(\tilde{\nu})$ alone. The reduction of the LB terms as a result of the DPM setup is seen in Eq. (15), where the β-LB terms are reduced by multiplying them by zeroth-order Bessel functions, and further cancelled by electronic subtraction, $i_{\mathrm{AC1}} - i_{\mathrm{AC2}}$ when the second PEM is properly adjusted such that $J_0[\delta^0_{M1}(\tilde{\nu})] = J_0[\delta^0_{M2}(\tilde{\nu})]$ and therefore that $J_1[\delta^0_{M1}(\tilde{\nu})] = J_1[\delta^0_{M2}(\tilde{\nu})]$ as well. However, the LB term, $-\varepsilon(\theta)\beta'_{\mathrm{M}}(\nu)\sin\theta$, in Eq. (15) still remains unaffected by the action of the second PEM. Frequently this LB term, which arises from the sample cell, is comparable to ΔA in magnitude and is only negligible under ideal conditions: the polarization axis of the detector is close to vertical and the polarization efficiency of the detector is very low. Otherwise, the effects of the remaining LB term may be significant, particularly when θ is close to 90° (polarization angle $\phi = 45°$) and $\beta'_{\mathrm{M}}(\nu)$ is large for a highly strained cell. The aim of introducing a RHWP is to further reduce this remaining LB term. This result also shows that in the absence of a sample cell, a properly aligned and adjusted DPM setup should yield a VCD baseline very close to zero, and in practice this has been found to be the case.

3.2 DPM setup with RHWP and one LB source

There are several choices of where the RHWP is placed on the optical train. It has been found theoretically, and also confirmed experimentally, that placing the RHWP behind the second PEM has the desired effect for LB reduction. The optical configuration of this setup is shown below:

$$S_{\mathrm{p}} \rightarrow \mathrm{PEM1} \rightarrow \mathrm{X} \rightarrow \mathrm{LB} \rightarrow \mathrm{PEM2} \rightarrow \mathrm{RHWP} \rightarrow \mathrm{DTC} \rightarrow S_{\mathrm{D}} \quad \text{(III)}$$

Similarly the final Stokes S_D vector can be obtained from the sequence of Mueller matrix operations

$$S_{\mathrm{D}} = M_{\mathrm{DTC}} M_{\mathrm{RHWP}} M_{\mathrm{PEM2}} M_{\mathrm{LB}} M_X M_{\mathrm{PEM1}} S_{\mathrm{P}} \quad (16)$$

The final intensity is determined by the following equation,

$$\begin{aligned} i_{\mathrm{D}}(\nu) &= i_{\mathrm{DC}}(\nu) + i_{\mathrm{AC1}}(\nu) \\ &= 1 + 2\Delta A J_1\left[\delta^0_{\mathrm{M1}}(\nu)\right] \end{aligned} \quad (17)$$

where neither β nor β' LB term is present in the equation and all the LB items are eliminated by the RHWP. This shows the dramatic effectiveness of the RHWP in the reduction of LB artifacts introduced by sample cells. However, if the RHWP is placed after the sample but before the second PEM, we have a very different result of the final intensity

$$\begin{aligned} i_{\mathrm{D}}(\nu) &= i_{\mathrm{DC}}(\nu) + i_{\mathrm{AC1}}(\nu) + i_{\mathrm{AC2}}(\nu) \\ &= 1 + 2\Delta A J_1[\delta^0_{\mathrm{M1}}(\nu)] \\ &\quad + \{2\varepsilon\beta \cos\theta J_0[\delta^0_{\mathrm{M1}}(\nu)]\} J_1[\delta^0_{\mathrm{M2}}(\nu)] \end{aligned} \quad (18)$$

where the LB terms are not completely eliminated by RHWP but reduced in size by the zeroth-order Bessel function.

Moreover, this term also cannot be cancelled by real time electronic subtraction since i_{AC1} has only a pure VCD contribution. It appears that the LB term in Eq. (18) as i_{AC2} may disappear if the second PEM is turned off. This is true if the sample cell is the only source of LB presented on the optical train. However, for actual setups, LB may come from before the first PEM and after the second PEM, such as from the detector focusing lens or the detector window. It is for the purpose of suppressing these LB items that we have included the second PEM behind the sample in the optical train. If the second PEM is not used, an LB source after RHWP cannot be suppressed only by a RHWP as shown below.

3.3 Single polarization modulation (SPM) setup with RHWP and two LB sources

Considering two LBs from both the sample cell (LB1) before the RHWP and (LB2) between the RHWP and the detector, including the detector window, in a setup with a single PEM (SPM), we have:

$$S_p \rightarrow \text{PEM1} \rightarrow \text{X} \rightarrow \text{LB1} \rightarrow \text{RHWP} \rightarrow \text{LB2} \rightarrow \text{DTC} \rightarrow S_D \quad \text{(IV)}$$

The corresponding matrix representation for this setup is:

$$S_D = M_{DTC} M_{LB2} M_{RHWP} M_{LB1} M_X M_{PEM1} S_P \quad (19)$$

The final intensity $i_D(\nu)$ was calculated to be

$$\begin{aligned} i_D(\nu) &= i_{DC}(\nu) + i_{AC}(\nu) \\ &= 1 + \varepsilon(\beta_2 \cos\theta - \beta_2' \sin\theta)\beta_1 J_0[\delta^0_{M1}(\nu)] \\ &\quad + 2[\Delta A + \varepsilon(\beta_2 \cos\theta - \beta_2' \sin\theta)] J_1[\delta^0_{M1}(\nu)] \end{aligned} \quad (20)$$

It is clear in Eq. (20) that LB2 terms are present together with ΔA and cannot be reduced or eliminated by RHWP. In the DC part, there are some additional terms that are generally very small compared to unity and hence can be ignored. Thus, the RHWP by itself as an artifact reducing element is able to eliminate all contributions to the VCD spectrum from LB1 in advance of its location but has no effect on LB2 contributions from its location in the optical train. This effect is complementary to the effect of a second PEM in the beam, as shown below.

3.4 DPM Setup without RHWP and with two LB Sources

This optical setup is shown below as (V), where no RHWP is introduced and two LBs are present before and after the second PEM, respectively:

$$S_p \rightarrow \text{PEM1} \rightarrow \text{X} \rightarrow \text{LB1} \rightarrow \text{PEM2} \rightarrow \text{LB2} \rightarrow \text{DTC} \rightarrow S_D \quad \text{(V)}$$

Converting setup (V) to the representation of Stokes vectors and Muller matrices, we have

$$S_D = M_{DTC} M_{LB2} M_{PEM2} M_{LB1} M_X M_{PEM1} S_P \quad (21)$$

The final total intensity is given by

$$\begin{aligned} i_D(\nu) &= i_{DC}(\nu) + i_{AC1}(\nu) + i_{AC2}(\nu) \\ &= 1 + \varepsilon\left(\cos\theta - \beta_1\beta_2\cos\theta + \beta_1\beta_2' \sin\theta\right) \\ &\quad \times J_0\left[\delta^0_{M1}(\nu)\right] J_0\left[\delta^0_{M2}(\nu)\right] \\ &\quad + 2\left\{\Delta A + \varepsilon\beta_1' \sin\theta + \varepsilon\left[\beta_2' \sin\theta \right.\right. \\ &\quad \left.\left. - (\beta_1 + \beta_2)\cos\theta\right] J_0\left[\delta^0_{M2}(\nu)\right]\right\} J_1\left[\delta^0_{M1}(\nu)\right] \\ &\quad + 2\varepsilon\left[\beta_2' \sin\theta - (\beta_1 + \beta_2)\cos\theta\right] \\ &\quad \times J_0\left[\delta^0_{M1}(\nu)\right] J_1\left[\delta^0_{M2}(\nu)\right] \end{aligned} \quad (22)$$

It can be seen in Eq. (22) that introduction of a second PEM in the beam permits suppression of most of the LB1 and LB2 contributions through multiplication by the zeroth-order Bessel function and electronic subtraction. As mentioned above, and similar to setup (II), one LB1 term, $\varepsilon\beta_1' \sin\theta$, from between the two PEMs, typically from the sample cell, is unmodified by the presence of PEM2, either by reduction due to $J_0[\delta^0_{M2}(\nu)]$ in $i_{AC1}(\nu)$ or cancellation through a corresponding term in $i_{AC2}(\nu)$. As shown in setup (III), this LB term can be suppressed by introducing a RHWP in the DPM setup as discussed below.

3.5 DPM setup with RHWP and two LB sources

The dual PEM setup that includes a RHWP positioned behind the second PEM and two sources of linear birefringence is shown as

$$S_p \rightarrow \text{PEM1} \rightarrow \text{X} \rightarrow \text{LB1} \rightarrow \text{PEM2} \rightarrow \text{RHWP} \rightarrow \text{LB2} \rightarrow \text{DTC} \rightarrow S_D \quad \text{(VI)}$$

The final Stokes vector is represented as

$$S_D = M_{DTC} M_{LB2} M_{RHWP} M_{PEM2} M_{LB1} M_X M_{PEM1} S_P \quad (23)$$

and the total intensity at the detector is

$$\begin{aligned} i_D(\nu) &= i_{DC}(\nu) + i_{AC1}(\nu) + i_{AC2}(\nu) \\ &= 1 + \varepsilon\left(\beta_2\cos\theta - \beta_2' \sin\theta\right)\beta_1 \\ &\quad \times J_0\left[\delta^0_{M1}(\nu)\right] J_0\left[\delta^0_{M2}(\nu)\right] \\ &\quad + 2\left\{\Delta A + \varepsilon(\beta_2\cos\theta - \beta_2' \sin\theta) J_0\left[\delta^0_{M2}(\nu)\right]\right\} \\ &\quad \times J_1\left[\delta^0_{M1}(\nu)\right] + 2\varepsilon\left(\beta_2\cos\theta - \beta_2' \sin\theta\right) \\ &\quad \times J_0\left[\delta^0_{M1}(\nu)\right] J_1\left[\delta^0_{M2}(\nu)\right] \end{aligned} \quad (24)$$

As in Eq. (17) for the same setup when only one source of LB was considered, no contributions from LB1 appear since they are eliminated by the RHWP. Differential absorbance ΔA is present in the AC1 term, together with two LB2 terms. The AC2 term consists only of the same two LB2 terms that appear in AC1. These two sources of LB2 terms cancel when the two PEMs are properly adjusted and the signal from the second PEM is subtracted from that of the first PEM. As a result, the combination of the DPM setup and a RHWP placed after the second PEM suppresses all sources of LBs in the entire optical train. This is confirmed experimentally as described in the following section.

4 Results and discussion

To confirm the above theoretical conclusions, the VCD spectra of camphor in solution were measured at four different settings in the CH-stretching region: (a) DPM/RHWP, the DPM setup with a RHWP after the second PEM; (b) DPM, the DPM setup only; (c) SPM/RHWP, the SPM setup with a RHWP after the second PEM (second PEM off); and (d) SPM, the SPM setup only. Two sample cells of 0.05 and 0.10 mm pathlengths were used to verify the effectiveness of LB reduction for the various setups with different cells. Figure 1 shows the VCD, IR absorbance, and VCD noise spectra of camphor in the CH-stretching region using a 0.05 mm pathlength cell with the normal DPM setup without a RHWP [3,5]. The VCD spectrum (middle trace) was obtained by subtraction of two enantiomeric spectra and is displayed here as a standard for comparison. In all spectra displayed, a wide spectral region is shown to give a full perspective of the baseline on either side of the absorbance and VCD bands. Figure 2a–d shows the unsubtracted VCD spectra measured in a 0.10 mm cell with the four different optical setups for both camphor and the solvent CCl_4, shown as bottom traces. The upper traces are the solvent-subtracted VCD spectra obtained from the two bottom traces. Figure 2e displays the overlay of two enantiomer VCD spectra of camphor measured for the SPM setup, and the top trace is their spectral difference, divided by 2. Similar spectral data for the sample cell with 0.05 mm pathlength, with somewhat different artifact patterns, is not presented here but is available as Supplementary Material.

It is clear that the VCD spectra measured with DPM/RHWP have the best quality of VCD baselines and the least artifacts compared with the other three settings. The VCD negative–positive couplet near $3,000\,cm^{-1}$ in the unsubtracted VCD spectrum (Fig. 2a) shows the closest match with the standard VCD spectrum in Fig. 1. The VCD spectrum of CCl_4 shows a quite flat and nearly featureless baseline, which outside the sample absorbance region, overlays the unsubtracted VCD spectrum of *R*-camphor very well. The solvent subtracted VCD spectrum of camphor (top trace in Fig. 2a) is identical to the standard VCD (Fig. 1) within the noise level. In accordance with the above theoretical analysis, these measurements confirm that the combination of DPM and RHWP allows for an authentic VCD spectrum to be obtained via solvent correction, the common situation encountered in practice. On the other hand, the VCD spectrum obtained by DPM only is less satisfactory, even after solvent correction, as shown in Fig. 2b. The VCD couplet at $3,000\,cm^{-1}$ is incorrectly biased, the positive band is more pronounced. This observation shows directly the distorting effects from the sample cell. Nevertheless, except for a less balanced VCD couplet, the overall VCD spectrum obtained for the DPM setup shows close similarities to the standard one.

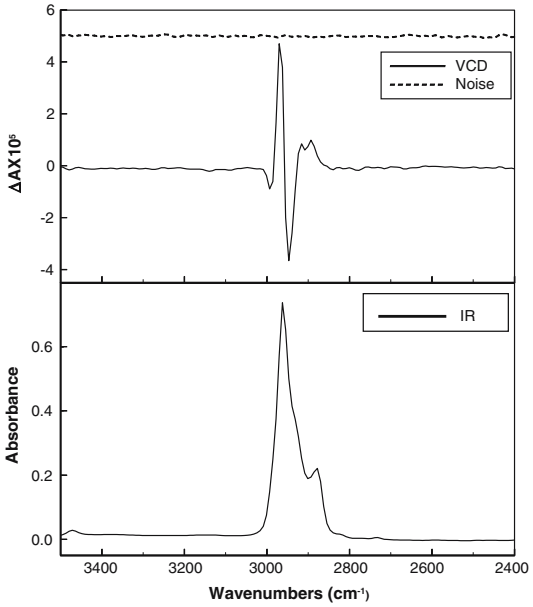

Fig. 1 VCD, IR, and VCD noise spectra of $(+)-(1R,4R)$-camphor in CCl4 (0.6 M) from about 4,000 to $2,000\,cm^{-1}$ region, measured in 0.05 mm cell. The VCD spectrum is one half the difference of the VCD spectrum of each enantiomer

The poorest setups for VCD measurements are shown in Fig. 2b, c, where the second PEM was not used for either of the two setups. This is not surprising, as it was demonstrated in our previous study [5] and also in the above theoretical description that the second PEM has a very substantial effect on the reduction of LB artifacts throughout the optical train, particularly before the first PEM and after the second PEM. Without the second PEM, the introduction of a RHWP on the optical train provides little improvement. This is clearly shown in the VCD spectrum in Fig. 2c, which was measured with the RHWP only. The raw VCD spectra of *R*-camphor and CCl_4 are very slanted (lower traces) such that the ordinate scale has to be changed from 10^{-5} to 10^{-4}. Within the larger scale, the VCD spectrum of *R*-camphor and CCl_4 seems to

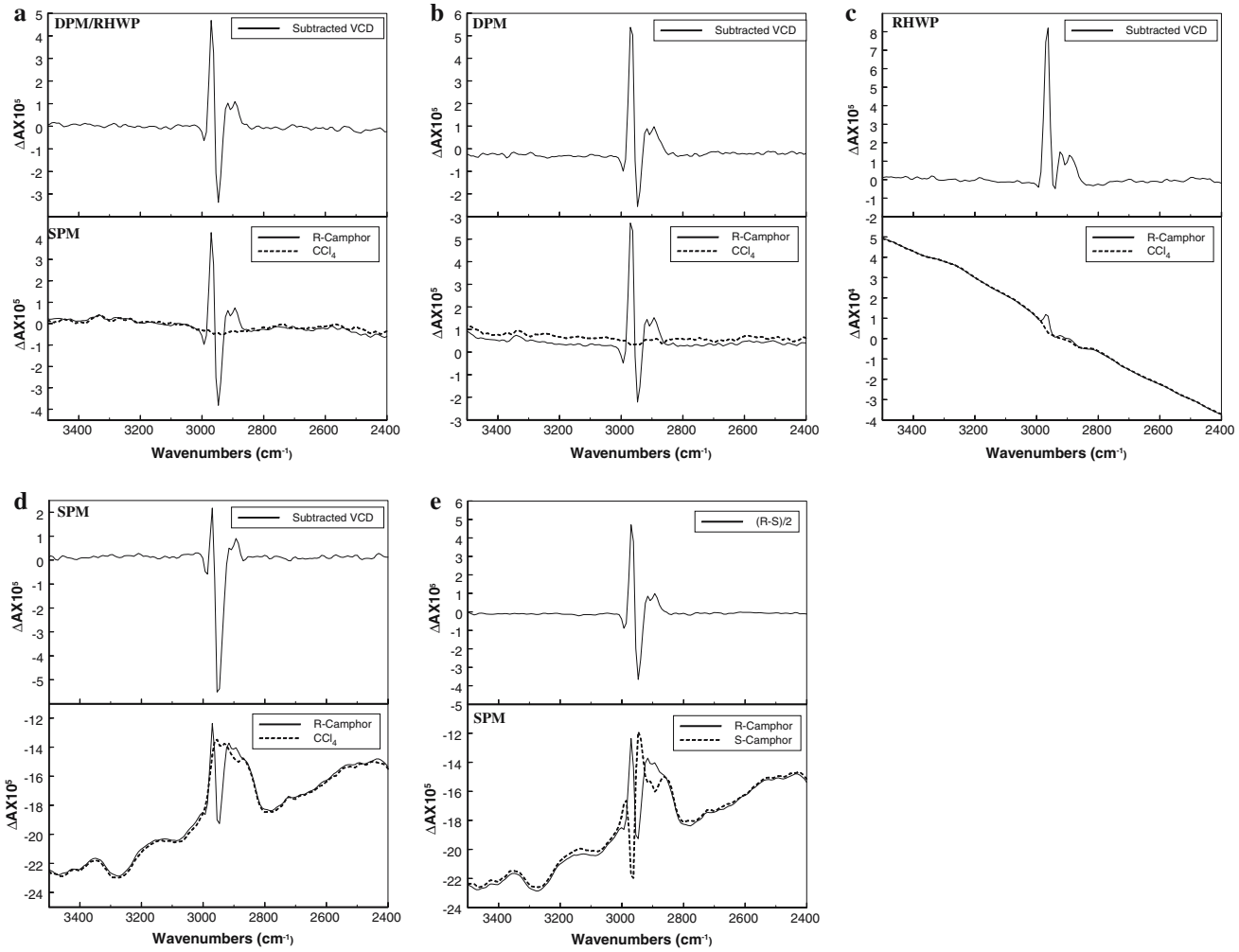

Fig. 2 Raw and subtracted VCD spectra of 0.6 M *R*-camphor in CCl_4 in a 0.10 mm CaF_2 cell from 4,000 to 2, 000 cm^{-1}: **a** DPM/RHWP, with both DPM and RHWP; **b** DPM, DPM only; **c** SPM/RHWP, single PEM (SPM) with RHWP; and **d** SPM, single PEM only; **e** SPM, single PEM only, for two enantiomers. The top traces are subtracted VCD spectra and the bottom traces are corresponding raw spectra

show a perfect overlay, but their subtracted spectra (upper trace) shows almost none of the negative part of the VCD couplet at 3, 000 cm^{-1}. Thus the VCD spectrum obtained at this setting is not reliable, even after the solvent correction.

The results obtained for the SPM setup are substantially different for the two sample cells although this difference is not shown here. With this setup, neither the second PEM nor the RHWP is used for the VCD measurement. The raw VCD spectra of *R*-camphor and CCl_4, shown as lower traces in Fig. 2d, are significantly different from the spectra obtained from all other setups. The VCD baseline for this setup is less slanted than that obtained with a RHWP, but it is located well below zero, indicating the presence of large LB artifacts. As Shown in Fig. 2d, the solvent subtracted spectrum (upper trace) is simply far away from the standard, the asymmetry of the couplet is almost reversed in sign and the negative band is much stronger than its positive partner. Clearly the single PEM setting is also unable to secure the measurement of an authentic VCD spectrum.

Figure 2e shows the VCD spectra obtained with the SPM setup for an overlay of spectra of *R*- and *S*-camphor (lower traces) and the subtracted spectrum of $(R - S)/2$ as upper trace. It is clear that although the raw VCD spectrum is seriously distorted and has a slanted and shifted baseline, the enantiomer-subtracted VCD spectrum is in excellent agreement with the standard VCD spectrum in Fig. 1. This is not surprising because the two enantiomers have the same absorbance and single-beam transmission spectra. However, as mentioned in the Introduction section, this ideal situation is not typical since often only one enantiomer is available so that solvent subtraction is the only choice for baseline correction.

In summary, we have shown theoretically and experimentally that the most effective setting for obtaining an authentic VCD spectrum from a sample of a single enantiomer is the

combination of DPM followed by a RHWP. The DPM setup is crucial for suppressing LB contributions throughout the optical train, and completely from LB sources before the first PEM and after the second PEM. The introduction of a RHWP behind the second PEM is able to further reduce the LB with birefringence axes at 45° from the PEM axes originating between the two PEMs, typically from sample cell windows. The setup DPM/RHWP consistently gives the highest quality VCD spectra for the two different sample cells. Although the VCD spectra from the DPM setup are less satisfactory, they are generally superior to those measured without the second PEM. The most slanted baselines were observed for the VCD spectra measured with a RHWP only, and serious artifacts were observed for both sample cells. The most severe artifacts are seen in the VCD spectrum measured with the single PEM setup, indicating the importance of adding the second PEM on the optical train. Here it should be pointed out that once the two PEMs have been aligned properly to achieve balanced cancellation and if the polarization sensitivity is low for the detector, adding a RHWP is not necessary to obtain accurate VCD spectra even for non-ideal sample cells. This has been demonstrated by our mid-infrared (2,000 to 800 cm^{-1}) FT-IR VCD spectrometer, where authentic VCD spectra have been obtained continually and universally without a RHWP. The FT-VCD spectrometer used for the present study operates in the high frequency region (4,000 to 2, 000 cm^{-1}) and is used for demonstration purposes without an optimum optical alignment. Clearly if the detector has some polarization sensitivity but a sample cell with negligible LB is used, it is also possible to obtain good quality VCD spectra without a RHWP. Thus, if a sample cell is not present on the optical train (empty bench), the VCD zero baseline measured with either the DPM/RHWP or DPM setups should theoretically have similar high quality with respect to baseline artifacts. Actually in this study the empty bench was used as the starting point for the initial light alignment and optical adjustments on the external optical train. Only when the VCD baseline is flat, close-to-zero and free of artifacts with no sample cell VCD measurements are carried out for real samples. To achieve this goal, the optical components of the DPM setup have to be carefully aligned and the retardation level of the second PEM has to be properly adjusted for complete LB cancellation. The final performance of the DPM setup or the combination of DPM and RHWP is largely affected by two factors: the size and shape of the infrared beam and the position of the two PEMs. To achieve the best performance, the positions of two PEMs have to be carefully adjusted for the optimal electronic LB cancellation. Perfect alignment is difficult to achieve in practice largely due to variations in the profile of the IR beam and differences in the degree of focus of the IR beam as it passes through each of the two PEMs. It can be seen that the raw VCD baselines of *R*-camphor and CCl_4 in Fig. 2a, b (lower traces) contain some minor features and they are not perfectly flat. Another source for this imperfection may be that the RHWP is treated as an ideal half-wave plate at all the points in the spectral region, and in practice there are small deviations from exact $\lambda/2$ retardation. Nevertheless, the DPM/RHWP setup removes nearly all background artifacts observed with the other setups, and for two of the setups, very large offsets are eliminated. Thus, the DPM/RHWP setup has clearly demonstrated its consistent and distinct effectiveness in obtaining the same authentic VCD spectrum of single enantiomers starting from a non-optimized VCD optical alignment.

5 Conclusions

The origin of poor baselines and artifacts in VCD spectra is predominantly linear birefringence. The LB originates in various sources, primarily the windows of the sample cell and detector and focusing lenses. The DPM setup plays an essential role in suppressing these LB terms and has been added to many mid-IR and near-IR FT-VCD spectrometers to provide excellent VCD spectra. With this setup, the LB terms in the calculated VCD spectra are reduced by multiplying them with a zeroth-order Bessel function and cancelled by real-time electronic subtraction. However, a remaining LB term due to LB located between the two PEMs, and with stress axes at 45° from the PEM axes, is not affected by the DPM setup and has a significant, adverse effect on VCD baselines with sample cells containing non-negligible LB. The introduction of a rotating half-wave plate placed behind the second PEM in the optical train is capable of eliminating this remaining LB term originating in the sample cell. Both the theoretical analysis and experimental measurements demonstrate that the DPM setup followed by a RHWP eliminates all sources of LB artifacts throughout the optical train. The DPM and RHWP are two complementary methods and their combination allows an accurate VCD spectrum to be obtained for single enantiomer after solvent correction, and to a good approximation without any correction whatsoever.

One limitation of this approach is finding a suitable achromatic wave plate for RHWP measurements beyond 2, 500 cm^{-1} into the mid-IR region. The possibility of using alternating plates of CdS and CdSe for coverage to 10 μm, 1, 000 cm^{-1} is currently being investigated. Such an extension of wavelength coverage would be welcome as most measurements of VCD are carried out in the mid-IR region between 2,000 and 800 cm^{-1}.

Acknowledgments Financial support from grants from the National Institutes of Health (GM 63148) and the National Science Foundation (CHE-0111402) are gratefully acknowledged.

References

1. Nafie LA, Freedman TB (2000) In: Circular dichroism: principles and applications, 2nd Ed. Nakanishi K, Berova N, Woody R (eds), Wiley-VCH, New York, pp 97
2. Nafie LA (1997) Ann Rev Phys Chem 48:357
3. Cao X, Shah RD, Dukor RK, Guo C, Freedman TB, Nafie LA (2004) Appl Spectrosc 58:1057
4. Nafie LA (1996) Appl Spectrosc 50:14A
5. Nafie LA (2000) Appl Spectrosc 54:1634
6. Cheng JC, Nafie LA, Stephens PJ (1975) J Opt Soc Am 65:1031
7. Lipp ED, Zimba CG, Nafie LA, Vidrine DW (1982) Appl Spectrosc 36:496
8. Malon P, Keiderling TA (1988) Appl Spectrosc 42:32
9. Polavarapu PL (1989) Appl Spectrosc 43:1295
10. Malon P, Keiderling TA (1996) Appl Spectrosc 50:669
11. Malon P, Keiderling TA (1997) Appl Opt 36:6141
12. Hug W (2003) Appl Spectrosc 57:1
13. Bailey J, Antonio C, Hough JH, Gledhill TM, McCall A, Clark S, Menard F, Tamura M (1998) Science 281:672
14. Hecht L, Barron LD, Blanch EW, Bell AF, Day LA (1999) Raman Spectrosc 30:815
15. Nafie LA, Buijs H, Rilling A, Cao X, Dukor RK (2004) Appl Spectrosc 58:647